

# Vortex signatures in annular Bose-Einstein condensates

M. Cozzini,<sup>1</sup> B. Jackson,<sup>1,2</sup> and S. Stringari<sup>1</sup>

<sup>1</sup>*Dipartimento di Fisica, Università di Trento and BEC-INFM, I-38050 Povo, Italy*

<sup>2</sup>*School of Mathematics and Statistics, Merz Court,  
University of Newcastle upon Tyne, NE1 7RU, United Kingdom*

(Dated: July 10, 2018)

We consider a Bose-Einstein condensate confined in a “Mexican hat” potential, with a quartic minus quadratic radial dependence. We find conditions under which the ground state is annular in shape, with a hole in the center of the condensate. Rotation leads to the appearance of stable multiply-quantized vortices, giving rise to a superfluid flow around the ring. The collective modes of the system are explored both numerically and analytically using the Gross-Pitaevskii and hydrodynamic equations. Potential experimental schemes to detect vorticity are proposed and evaluated, which include measuring the splitting of collective mode frequencies, observing expansion following release from the trap, and probing the momentum distribution of the condensate.

PACS numbers: 03.75.Lm, 03.75.Kk, 67.40.Vs

## I. INTRODUCTION

The 1995 discovery of Bose-Einstein condensation in dilute ultracold gases [1, 2, 3] prompted a flurry of activity investigating these fascinating quantum systems. In the experiments, ultracold atoms are confined by magnetic or optical forces, which typically can be represented theoretically by a harmonic potential. Lately, however, an increasing amount of interest has focused on Bose condensates in more exotic trapping potentials. For example, Gupta *et al.* [4] recently produced a condensate in a ring-shaped magnetic waveguide, while experiments at Ecole Normale Supérieure [5, 6] have been conducted in overlapping magnetic and optical dipole traps, leading to a potential which can be approximated by a function which is quadratic plus quartic in the radial coordinate. This trap potential is especially of interest when the condensate is rotating, since, in contrast to the harmonic case, one can in principle achieve arbitrarily high angular velocities. This leads to interesting new configurations, for example a vortex lattice with a hole at its center, and for even higher angular velocities, annular condensates containing a multiply-quantized “macrovortex”. These equilibrium configurations have been studied in a number of papers [7, 8, 9], where the angular velocities for transitions between the different states, defining a phase diagram, were calculated in Refs. [10, 11, 12, 13, 14]. In addition to the static properties, the dynamics have also been addressed, with the collective mode excitations considered in Refs. [13, 15].

Alternatively, one could consider the case where, in addition to the quartic term, there is a *negative* harmonic term. Then the radial trap potential has the form of a “Mexican hat”, and the condensate can be annular even when there is no rotation. Similar trap configurations have been studied elsewhere [16, 17, 18, 19]. Of particular interest, however, is the behavior of the system under rotation, since vortices can enter the condensate and form a stable, multiply-quantized vortex at the center. For example, an important question raised in this configura-

tion concerns the stability of the vortex in the presence of a non-rotating thermal cloud at finite temperatures—does the vortex decay by spiraling towards the edge as in a harmonic trap [20, 21], or is it metastable? This is related to the well-known problem of stability of persistent currents in superfluids [22, 23], and so is of interest from a fundamental perspective.

In order to tackle these types of questions experimentally it is important to possess some way of detecting the presence of a vortex. In a harmonically-trapped condensate this is relatively straightforward, since the fluid circulation around the vortex core creates a hole in the density, which can be detected by standard absorption imaging. Since the optical resolution is usually not sufficient to detect vortices *in situ*, a period of free expansion following the release of the condensate from the trap is generally required. However, in a trapped annular condensate vortices reside in the center where the density is very low irrespective of the circulation. Hence, imaging of a vortex *in situ* is precluded, and it is not even obvious *a priori* whether it is possible to resolve the vortex after expansion. A more detailed analysis is thus required in order to evaluate the feasibility of this and other possible schemes for vortex detection.

In this paper we shall study two-dimensional condensates, where the trap potential has a quartic minus quadratic radial dependence. Most of our results for thin annular condensates, however, also apply to more general Mexican hat potentials. Two dimensions in this context corresponds to either a cylindrical condensate, where the axial length scale greatly exceeds the radial size, or a thin disk-shaped condensate where the system is tightly trapped in the axial direction such that dynamics along this coordinate are “frozen out” and can be neglected. Both geometries are of experimental interest. We also focus exclusively on condensates in the mean field regime at zero temperature, where the properties can be accurately described by the Gross-Pitaevskii (GP) equation. Nevertheless, we should mention that the possibility of obtaining a thin annulus, essentially a one-dimensional

system, opens up other interesting regimes beyond mean field, such as a quasi-condensate or Tonks-Girardeau gas [24].

We begin by studying the equilibrium states, where both numerical solutions and analytical results are presented. We then characterize the lowest energy excitations, or collective modes, of the condensate. In particular, we use a hydrodynamic model to derive analytical expressions in the limit of thin annuli, as well as to find the mode frequencies numerically. We also compare these results to numerical simulations of the GP equation. This allows us to discuss the use of collective modes to detect vorticity; namely the splitting between counter-propagating surface and acoustic modes of the condensate. We then consider the expansion of the condensate after switching off the confining potential, finding that the hole due to the vortex is recovered in the expanded density, providing a simple means to detect the presence of the vortex in experiments. Finally, we discuss the momentum distribution of an annular condensate, finding that in the limit of thin annuli the function approaches a simple analytical form.

## II. EQUILIBRIUM CONFIGURATIONS

For a dilute Bose-Einstein condensate in the limit of zero temperature, the time-dependent evolution of the condensate wavefunction  $\Psi(\mathbf{r}, t)$  is described by the Gross-Pitaevskii (GP) equation

$$i\hbar \frac{\partial \Psi}{\partial t} = \left( -\frac{\hbar^2}{2M} \nabla^2 + V_{\text{ext}} + g_{3D} |\Psi|^2 \right) \Psi. \quad (1)$$

The interactions between atoms are represented by the parameter  $g_{3D} = 4\pi N \hbar^2 a / M$ , for  $N$  atoms of mass  $M$ , with  $s$ -wave scattering length  $a$ . Note that, in addition to the dynamics of the condensate, the time-independent stationary states can be found by substituting  $\Psi(\mathbf{r}, t) = \Psi(\mathbf{r}) e^{-i\mu t / \hbar}$  into Eq. (1), whereupon the left-hand side becomes  $\mu \Psi$  with  $\mu$  the chemical potential. The external potential in Eq. (1) is of the form

$$V_{\text{ext}}(\mathbf{r}) = \frac{\hbar \omega_{\perp}}{2} \left( \sigma \frac{r^2}{d_{\perp}^2} + \lambda \frac{r^4}{d_{\perp}^4} \right) + \frac{\hbar \omega_z}{2} \frac{z^2}{d_z^2}, \quad (2)$$

where  $d_i = \sqrt{\hbar / (M \omega_i)}$ , with  $\omega_{\perp}$  and  $\omega_z$  the radial and axial trap frequencies respectively. In the following we shall mostly use harmonic oscillator units where distance, time and energy are expressed in units of  $d_{\perp}$ ,  $\omega_{\perp}^{-1}$  and  $\hbar \omega_{\perp}$  respectively. We also take  $\sigma = -1$ , where the case of  $\sigma = 1$  has already been extensively studied in a number of papers [7, 8, 9, 10, 11, 12, 13, 14, 15].

We explicitly consider the GP equation in 2D

$$i \frac{\partial \Psi}{\partial t} \Psi = \left[ -\frac{1}{2} \nabla^2 + \frac{1}{2} (-r^2 + \lambda r^4) + g |\Psi|^2 \right] \Psi, \quad (3)$$

where the evolution in the axial coordinate is neglected. Physically this can correspond to the case of a cylindrical condensate, where  $\omega_z \ll \omega_{\perp}$ . The interaction parameter then becomes,  $g = 4\pi N' a$ , in harmonic oscillator units, where  $N' = N/Z$  represents the number of atoms per unit length along the axial direction. An alternative two-dimensional configuration involves tight axial confinement, such that  $\hbar \omega_z \gg g_{3D} |\Psi(0)|^2$  in physical units. In this geometry, which has been realized experimentally [25], the axial dynamics are ‘‘frozen out’’. The axial dependence of the wavefunction is then gaussian, and the 2D GP equation (3) can be used with  $N' = N / (\sqrt{2\pi} d_z)$  [26].

We first analyze a condensate without a vortex using the Thomas-Fermi (TF) approximation, where the spatial derivative of  $\Psi$  in Eq. (3) is neglected, so that the density is given by  $n(\mathbf{r}) \equiv |\Psi(\mathbf{r})|^2 = (\mu - V_{\text{ext}}) / g$  for  $n(\mathbf{r}) > 0$ , and  $n(\mathbf{r}) = 0$  otherwise. The radii of the condensate are evaluated by finding where the density goes to zero. If  $\mu > 0$  then there is a single solution of the resulting quadratic equation,  $R^2 = (1 + \sqrt{1 + 8\lambda\mu}) / (2\lambda)$ , which corresponds to a condensate without a hole. On the other hand, if  $\mu < 0$  there are two solutions  $R_{1,2}^2 = (1 \mp \sqrt{1 + 8\lambda\mu}) / (2\lambda)$ , and the condensate is annular with a hole in the center. In this case one can write the TF condensate density as

$$n(\mathbf{r}) = \frac{\lambda}{2g} (R_2^2 - r^2)(r^2 - R_1^2), \quad (4)$$

for  $n(\mathbf{r}) > 0$ . Calculating the radii and chemical potential more explicitly requires the condition that the wavefunction is normalized to unity  $\int d\mathbf{r} n(\mathbf{r}) = 1$ . The resulting radii can be conveniently expressed as the sum and difference of the squares  $R_{\pm}^2 = R_2^2 \pm R_1^2$ , yielding

$$\lambda R_+^2 = 1, \quad (5)$$

$$\lambda R_-^2 = \eta \equiv \left( \frac{12g\lambda^2}{\pi} \right)^{1/3}, \quad (6)$$

where we have defined a new parameter  $\eta$  in Eq. (6). The chemical potential is then

$$\mu = \frac{\eta^2 - 1}{8\lambda}. \quad (7)$$

This yields the condition  $\eta < 1$  for an annular condensate, which we will always assume in the following. The limit  $\eta \rightarrow 0$  corresponds to the case where the width of the annulus becomes much smaller than the radius.

The range of validity of the TF approximation for an annular condensate is defined by the condition  $\xi \ll d$  [12], where  $\xi = (2gn_{\text{max}})^{-1/2}$  is the healing length at the density maximum, while  $d = R_2 - R_1$  is the width of the annulus. Using the above expressions yields the explicit relations  $\xi = 2\sqrt{\lambda} / \eta$  and  $d = (\sqrt{1 + \eta} - \sqrt{1 - \eta}) / \sqrt{2\lambda}$ .

The condensate can also contain a single centered vortex with circulation  $\Gamma = 2\pi\nu\hbar/M$ , where the well-known

requirement of quantized circulation in superfluids [27] constrains the vorticity to integer values  $\nu = 0, 1, 2, \dots$ . The equilibrium condensate density is represented within the TF approximation as

$$gn(\mathbf{r}) = \mu - \frac{1}{2} \left( \frac{\nu^2}{r^2} - r^2 + \lambda r^4 \right), \quad (8)$$

where  $\mu$  is the chemical potential in the laboratory (non-rotating) frame and the  $\nu^2/r^2$  term corresponds to the centrifugal potential barrier resulting from the fluid flow around the vortex. Performing an analysis similar to that of the non-rotating condensate gives the following relations

$$(\lambda\nu)^2 = \frac{(\lambda R_+^2 - 1)[(\lambda R_+^2)^2 - (\lambda R_-^2)^2]}{4}, \quad (9)$$

$$\lambda\mu = \frac{1}{2} \left[ \frac{3(\lambda R_+^2)^2 + (\lambda R_-^2)^2}{4} - \lambda R_+^2 \right], \quad (10)$$

$$\frac{\eta^3}{12} = \frac{2}{3} \lambda^2 \mu R_-^2 - \frac{(\lambda\nu)^2}{2} \ln \left( \frac{R_+^2 + R_-^2}{R_+^2 - R_-^2} \right) + \frac{\lambda^2 R_+^2 R_-^2}{12}. \quad (11)$$

Approximate analytical solutions of Eqs. (9-11) can be obtained using the expansion  $\lambda R_+^2 = 1 + \sum_n c_n (\lambda\nu)^{2n}$ , which is most appropriate for  $\lambda\nu \ll 1$ . As we shall see this regime is the most interesting for our purposes, since it corresponds to the region where a multiply-quantized vortex is stable. Substituting into Eqs. (9-11) yields the following results

$$\lambda R_+^2 = 1 + \frac{4}{1 - \eta^2} (\lambda\nu)^2 + \mathcal{O}[(\lambda\nu)^4], \quad (12)$$

$$\lambda R_-^2 = \eta + \frac{1}{\eta} \left[ \frac{4}{\eta^2 - 1} + \frac{2}{\eta} \ln \left( \frac{1 + \eta}{1 - \eta} \right) \right] (\lambda\nu)^2 + \mathcal{O}[(\lambda\nu)^4], \quad (13)$$

$$\lambda\mu = \frac{\eta^2 - 1}{8} + \frac{1}{2\eta} \ln \left( \frac{1 + \eta}{1 - \eta} \right) (\lambda\nu)^2 + \mathcal{O}[(\lambda\nu)^4]. \quad (14)$$

Another important quantity is the energy of the condensate in the presence of a vortex. This is represented in terms of an energy per particle as an integral

$$E = \frac{1}{2} \int d\mathbf{r} \Psi^* (-\nabla^2 - r^2 + \lambda r^4 + gn) \Psi. \quad (15)$$

Within the TF approximation the energy becomes

$$E = \frac{1}{2} \int d\mathbf{r} \left( \frac{\nu^2}{r^2} - r^2 + \lambda r^4 + gn \right) n. \quad (16)$$

Eq. (16) can be approximated analytically using the TF density (8) and the expansions (12-14). This eventually yields

$$\lambda E = -\frac{1}{8} + \frac{3}{40} \eta^2 + E_1 (\lambda\nu)^2 + \mathcal{O}[(\lambda\nu)^4], \quad (17)$$

where we have defined the second-order term separately

$$E_1 = \frac{3}{4\eta^3} \left[ 2\eta - (1 - \eta^2) \ln \left( \frac{1 + \eta}{1 - \eta} \right) \right]. \quad (18)$$

Interestingly, this term can also be derived by calculating the kinetic energy from the circulation of the vortex  $\int d\mathbf{r} n\nu^2/(2r^2)$ , where  $n$  is approximated by the density without a vortex (4).

The energy in a frame rotating with angular velocity  $\Omega$  is related to that in the laboratory frame by  $E'(\nu) = E(\nu) - \Omega\nu$ . For a particular  $\Omega$  there exists a vorticity  $\nu$  that minimizes this energy, identifying the ground state for each rotation rate. Treating  $\nu$  as a continuous quantity (valid for  $\nu \gg 1$ ) and using Eq. (17) to second order gives the following condition for the ground state vorticity

$$\lambda\nu = \frac{\Omega}{2E_1}. \quad (19)$$

In the limit  $\eta \rightarrow 0$  this expression becomes particularly simple, since  $E_1 \simeq 1$ , so that  $\lambda\nu \simeq \Omega/2$ . This can also be easily derived by equating the velocity due to the rotation at the radius of the annulus,  $v = \Omega R$ , to the fluid velocity due to the vortex,  $v = \nu/R$ , where  $R^2 = R_+^2/2 = 1/(2\lambda)$ .

These analytical results can be compared to solutions of the GP equation in the rotating frame

$$i \frac{\partial}{\partial t} \Psi = \left[ -\frac{1}{2} \nabla^2 + \frac{1}{2} (-r^2 + \lambda r^4) + g|\Psi|^2 - \Omega \hat{L}_z \right] \Psi, \quad (20)$$

where  $\hat{L}_z = i(y\partial/\partial x - x\partial/\partial y)$  is the axial component of the angular momentum operator. To find the equilibrium configuration for each  $\Omega$  we solve Eq. (20) numerically by propagating in imaginary time (i.e. making the replacement  $t \rightarrow -it$ ), starting from the  $\Omega = 0$  ground state.

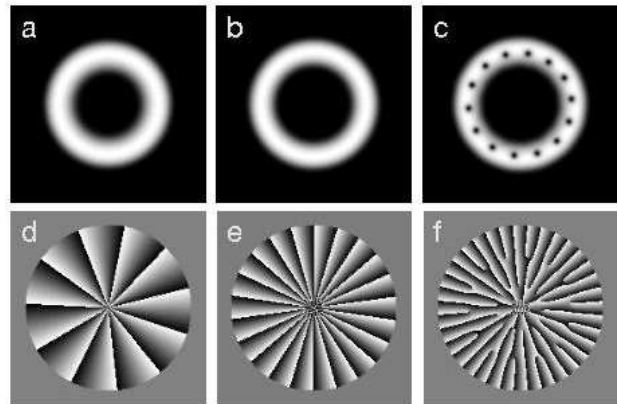


FIG. 1: Density profiles of a condensate, found by numerical solution of the GP equation (20) with  $g = 1000$  and  $\lambda = 0.01$  ( $\eta = 0.726$ ) for (a)  $\Omega = 0.2$  (in units of  $\omega_\perp$ ), (b)  $\Omega = 0.4$ , and (c)  $\Omega = 0.5$ ; (d)-(f) show the corresponding phase profiles for each  $\Omega$ . The length scale of each box is  $28 \times 28$  (in units of  $d_\perp$ ).

This technique yields the configurations shown in Fig. 1. One can write the condensate wavefunction as  $\Psi(\mathbf{r}) = \sqrt{n(\mathbf{r})} \exp[iS(\mathbf{r})]$ , where  $n(\mathbf{r}) = |\Psi(\mathbf{r})|^2$  is the density and  $S(\mathbf{r})$  is the phase. Fig. 1 shows the density and phase at three different rotation rates for a particular set of parameters ( $g = 1000$ ,  $\lambda = 0.01$ ,  $\eta = 0.726$ ). For  $\Omega = 0.2$  (Fig. 1(a)) the equilibrium state consists of a stable multiply-quantized vortex with  $\nu = 11$ , as can be seen from plotting the phase (Fig. 1(d)) where, by traversing the center in a closed loop, one finds 11 cycles between  $S = 0$  (black) and  $S = 2\pi$  (white). At  $\Omega = 0.4$  (Figs. 1(b) and (e)) the multiply-quantized vortex is again stable, but with  $\nu = 22$ . However, at  $\Omega = 0.5$  (Figs. 1(c) and (f)) a multiply-quantized vortex at the center of the condensate is surrounded by two rings of singly-quantized vortices. The outer ring is visible in the density plot since the vortices are embedded in the condensate. This transition between a “macrovortex” and a “lattice with hole” state was previously found in Ref. [19] for 3D configurations. This is similar to the transition in quartic plus quadratic traps discussed in Refs. [10, 11, 12, 13, 14], except that in the latter case the transition takes place at a much higher frequency and in the opposite direction. To find the critical rotation rate for the transition in the present configuration would require a detailed analysis, possibly using techniques similar to Refs. [13, 14].

In the remainder of the paper we shall focus on the macrovortex state, (i.e. one where there is a single, multiply-quantized vortex in the center of the hole) where in all cases we have checked that the macrovortex is stable in the rotating frame by numerically solving the GP equation. The analytical results derived above can then be used, and compared to numerical solutions of the GP equation. In order to facilitate such a comparison, it is simpler to solve the GP equation in the non-rotating frame with an effective potential  $V_{\text{ext}}(r, z = 0) + \nu^2/(2r^2)$ . The energy can then be calculated from the density using Eq. (15) and is compared to the analytical expression (17) in Fig. 2. One sees good agreement for  $\nu < 20$  (corresponding to  $\lambda\nu < 0.2$ ), which is the region where Eq. (17) is expected to be valid. To find the ground state for a particular rotation rate  $\Omega$  one can, as before, simply identify the  $\nu$  that minimizes the rotating frame energy  $E'(\nu) = E(\nu) - \nu\Omega$ . The resulting  $\nu$  vs.  $\Omega$  plot is compared to the analytical result (19) in the inset of Fig. 2, again showing good agreement for small  $\lambda\nu$ .

Before continuing, it is interesting to relate our work to more general “Mexican hat” type potentials—for example, a harmonic plus gaussian potential [18] which experimentally would correspond to magnetic trap overlaid with a tightly-focussed blue-detuned laser beam. In particular, for a thin annulus, when the condensate is confined close to the potential minimum at radius  $R$ , the radial trap potential can be expanded to second order in  $r - R$  as

$$V(r) = \frac{M}{2} \omega_r^2 (r - R)^2 + \mathcal{O}[(r - R)^3] \quad (21)$$

where we have neglected a constant term which does

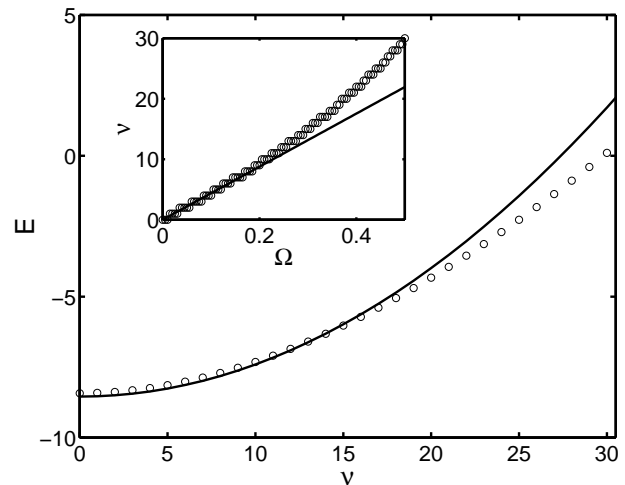


FIG. 2: Energy (in units of  $\hbar\omega_{\perp}$ ) of the condensate with a central vortex as a function of vorticity  $\nu$  for the same parameters as Fig. 1. The circles plot numerical solutions of the GP equation, while the solid line is the analytical estimate (17). *Inset:* vorticity of the ground state in a frame rotating with angular velocity  $\Omega$  (in units of  $\omega_{\perp}$ ). Circles are numerical GP solutions, while the solid line plots the analytical result (19).

not affect the dynamics. For our potential (2) we find  $\omega_r = \sqrt{2}\omega_{\perp}$  and  $R = d_{\perp}/\sqrt{2\lambda}$  (in physical units). In the following, the results presented for the thin annulus limit  $\eta \ll 1$  are therefore applicable to more general potentials, where finding  $\omega_r$  and  $R$  from the corresponding expansion (21) allows a precise mapping onto our system.

### III. COLLECTIVE MODES

In the previous section it was found that, within the TF approximation, a hole is present within a non-rotating condensate for  $\eta < 1$ . Considering a condensate rotating with sufficiently small angular velocities  $\Omega$ , we found equilibrium configurations where multiply-quantized vortices are stable. An interesting question concerns how these vortices could be detected experimentally, since the density profiles of a condensate with no vortex or small values of  $\nu$  are very similar, making it very difficult to distinguish between the different states on this basis alone. One possibility is to study the collective modes of the system, since differences in the vorticity may be manifested in the frequencies, in a similar way to those in a harmonic trap [28, 29, 30]. The problem of collective modes in annular condensates is also interesting in its own right, as similar investigations in a rapidly rotating quadratic plus quartic trap have shown [15]. This section will therefore detail similar analyses for a quartic minus quartic confinement, with the specific application to vortex detection discussed at the end.

One approach to finding collective mode frequencies is

to rewrite the GP equation in the rotating frame (20) in terms of the density and phase, and use the TF approximation to obtain hydrodynamic equations for these quantities. Then linearizing for small fluctuations about equilibrium,  $\delta S$ ,  $\delta n$ , yields

$$\frac{\partial}{\partial t} \delta n + \left( \frac{\nu}{r^2} - \Omega \right) \frac{\partial \delta n}{\partial \phi} + \nabla \cdot (n_0 \nabla \delta S) = 0, \quad (22)$$

$$\frac{\partial}{\partial t} \delta S + \left( \frac{\nu}{r^2} - \Omega \right) \frac{\partial \delta S}{\partial \phi} + g \delta n = 0, \quad (23)$$

where  $n_0$  is the TF equilibrium density from Eq. (8). For density and phase modulations of the form  $\delta n, \delta S \propto e^{i(m\phi - \omega t)}$  this gives  $\delta n = i(\omega + m\Omega - m\nu/r^2)\delta S$  and

$$\left[ \left( \omega + m\Omega - \frac{m\nu}{r^2} \right)^2 - \frac{m^2}{r^2} g n_0 \right] \delta S + \frac{1}{r} \frac{\partial}{\partial r} \left( r g n_0 \frac{\partial}{\partial r} \delta S \right) = 0, \quad (24)$$

where  $\omega$  is the frequency of the mode in the rotating frame.

It is instructive to first consider the case of a non-rotating condensate where  $\Omega = 0$  and  $\nu = 0$ . Similarly to Ref. [15], one can introduce the new variable  $\zeta = (r^2 - R_+^2/2)/(R_-^2/2)$ , so that the equilibrium density (4) becomes  $g n_0 = \lambda R_-^4 (1 - \zeta^2)/8$  and  $-1 \leq \zeta \leq 1$ . Substituting into Eq. (24) then gives

$$\left( \omega^2 - \frac{m^2 \eta^2}{4} \frac{1 - \zeta^2}{1 + \eta \zeta} \right) \delta S + \frac{\partial}{\partial \zeta} \left[ (1 + \eta \zeta)(1 - \zeta^2) \frac{\partial}{\partial \zeta} \delta S \right] = 0. \quad (25)$$

Note that this equation, and therefore the mode frequency, depends only upon the parameter  $\eta$  and the square of the azimuthal quantum number  $m$ , the positive and negative  $m$  modes being degenerate for symmetry reasons. In the limit of  $\eta \rightarrow 0$  (i.e. when the width of the annulus is small compared to its radius, as evident from the relation  $\eta = R_-^2/R_+^2$ ) the equation becomes

$$\omega^2 \delta S + \frac{\partial}{\partial \zeta} \left[ (1 - \zeta^2) \frac{\partial}{\partial \zeta} \delta S \right] = 0, \quad (26)$$

which is Legendre's equation with eigenfunctions given by Legendre polynomials  $P_j(\zeta)$  and eigenvalues  $\omega^2 = j(j+1)$ , where  $j = 0, 1, 2, \dots$  is the number of radial nodes [31]. Hence, different  $m$  states are degenerate in this limit [32]. The same result for the frequencies can also be derived starting from the expanded potential (21) with the corresponding one-dimensional hydrodynamic equation for the radial coordinate. This implies that the modes can be pictured as consisting of different parts of the annular condensate undergoing radial oscillations in a one-dimensional harmonic well, providing a simple explanation for the mode frequencies and the degeneracy of different  $m$  states.

Apart from these analytical considerations, one can also solve Eq. (25) numerically using a shooting method [33] to find the mode frequencies  $\omega$  and functions  $\delta S(\zeta)$ . Fig. 3(a) shows the high-lying ( $j = 1$ )  $m = 0, 1, 2$  mode frequencies as a function of  $\eta$  for the non-rotating ( $\Omega = 0$ ,  $\nu = 0$ ) condensate in the presence of the hole ( $\eta < 1$ ). One sees that in the limit of  $\eta \rightarrow 0$  all of the mode frequencies tend to  $\omega = \sqrt{2}$ , consistent with the above analysis. With increasing  $\eta$ , however, the frequencies deviate from this value, with a particularly marked decrease in the  $m = 0$  mode as one approaches  $\eta = 1$ . In addition, it becomes increasingly difficult to find numerical solutions near to  $\eta = 1$ . Numerical results from simulating the time-dependent GP equation (3) for each mode are also presented in Fig. 3(a). The GP results closely follow the hydrodynamic equations up to  $\eta = 0.7$ , above which the GP results start to deviate significantly. This discrepancy is related to the fact that when the inner radius approaches zero at  $\eta \rightarrow 1$  the contrast between the density profiles for the TF approximation (where the density goes to zero suddenly) and from solving the GP equation (where the density tails off more gradually) becomes increasingly significant, leading to differences in the nature of the modes near to the center. In addition, the transition between hole and non-hole states in the GP solution is more gradual, avoiding the singular behavior in the hydrodynamic equation at  $\eta = 1$ .

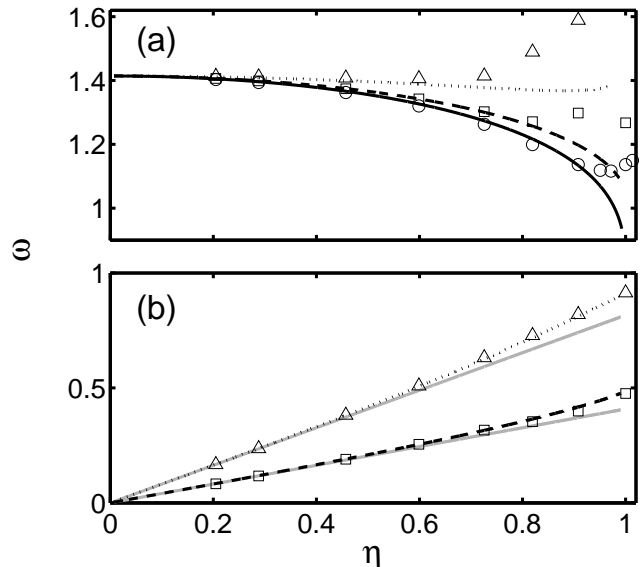


FIG. 3: (a) Frequency (in units of  $\omega_{\perp}$ ) of the high-lying ( $j = 1$ )  $m = 0$  (solid line)  $m = 1$  (dashed) and  $m = 2$  (dotted) modes as a function of  $\eta$  for a non-rotating condensate ( $\Omega = 0$ ), from numerical solution of the hydrodynamic equation (25). Also plotted are numerical solutions of the Gross-Pitaevskii equation (3) at  $g = 1000$  for  $m = 0$  ( $\circ$ ),  $m = 1$  ( $\square$ ) and  $m = 2$  ( $\triangle$ ). (b) Frequencies of the low-lying ( $j = 0$ )  $m = 1$  and  $m = 2$  modes, where the grey lines show the analytical result (28) for each  $m$ , while the other lines and points are labelled similarly to (a).

The low-lying ( $j = 0$ )  $m > 0$  modes can also be investigated, and the  $m = 1$  and  $m = 2$  modes frequencies are plotted as a function of  $\eta$  in Fig. 3(b). Comparison between the hydrodynamic and GP results again show very good agreement. Similar modes were found in a rapidly rotating quadratic plus quartic traps in Ref. [15], and in the thin annulus limit  $\eta \ll 1$  correspond to compressional modes directed azimuthally around the annulus, in contrast to the high-lying modes which correspond to shape oscillations of the annulus. This physical explanation is the basis of a simple analysis, starting from the relation  $\omega = cq$ , where for a narrow annulus  $q = m/R$ , with the mean radius  $R = R_+/\sqrt{2}$ . The speed of sound,  $c$ , is given by the relation  $c^2 = n_1 \partial\mu/\partial n_1$ , where  $n_1 = N'/(2\pi)$  is the density of the condensate integrated over the radial direction. Rewriting in terms of  $\eta$  yields the equation

$$\omega^2 = \frac{2m^2}{3\lambda R_+^2} \eta \frac{\partial}{\partial \eta} (\lambda\mu). \quad (27)$$

Substituting Eqs. (5) and (7) for a non-rotating condensate,  $\lambda\nu = 0$ , gives  $c = \eta/\sqrt{12\lambda}$  and

$$\omega = |m| \frac{\eta}{\sqrt{6}}. \quad (28)$$

The mode frequencies for  $m = 1$  and  $m = 2$  found from Eq. (28) are plotted as a function of  $\eta$  in Fig. 3(b). This analytical estimate is exact for thin annuli [32], and indeed the comparison to the hydrodynamical results shows excellent agreement for  $\eta < 0.4$ .

So far we have only studied the non-rotating case where  $\Omega = 0$ . In a frame rotating with a non-zero angular frequency,  $\Omega \neq 0$ , we demonstrated earlier that for sufficiently small  $\Omega$  the ground state consists of a multiply quantized vortex  $\nu > 1$ . These stationary states can be described analytically within the TF approximation using Eq. (8) for the density. From the normalization condition for the density one can find the chemical potential and energy for each  $\nu$ , followed by the  $\nu$  state which minimizes the energy in a frame rotating with frequency  $\Omega$ . Substituting the resulting  $\nu$  and  $n_0$  into Eq. (24) and solving numerically then yields mode frequencies for this particular  $\Omega$ .

We find that the rotating-frame frequencies for the high-lying ( $j = 1$ ) modes change significantly with increasing  $\Omega$ , with a rather large splitting between  $m = +|m|$  and  $m = -|m|$  modes for a given  $|m| > 0$ . In contrast, the  $\Omega$  dependence of the low-lying ( $j = 0$ ) mode frequencies is less pronounced, and is almost independent of the sign of  $m$ . In the laboratory frame, however, one has a frequency splitting between low-lying modes of opposite  $m$ . Using a sum rule analysis similar to that of Ref. [28] gives for this splitting

$$\Delta\omega = 4|m|\lambda\nu[1 + \mathcal{O}(\eta^2)], \quad (29)$$

where a similar expression was derived using perturbation theory in Ref. [18] for a thin toroid in a quadratic

plus gaussian potential. For the thin annulus ( $\eta \ll 1$ ) one can use Eqs. (28) and (29) to derive a simple equation for the frequencies of the low-lying modes in the laboratory frame

$$\omega_{\pm} = |m| \left( \frac{\eta}{\sqrt{6}} \pm 2\lambda\nu \right). \quad (30)$$

Note that these expressions can also be derived by using the quasi-degeneracy between modes in the rotating frame, together with the transformation  $\omega_{\text{lab}} = \omega_{\text{rot}} + m\Omega$  and Eq. (19) with  $E_1 \simeq 1$ .

In Fig. 4(a) we plot the laboratory-frame frequencies,  $|\omega_{\text{lab}}|$ , of the  $m = \pm 2$  low-lying modes as a function of  $\nu$  and  $\Omega$  for a thin annulus, where  $\lambda = 0.00322$ ,  $g = 680$ , and  $\eta = 0.3$ . To place these values into physical context, note that they would correspond to e.g.  $10^6$   $^{87}\text{Rb}$  atoms in a cylindrical condensate  $100 \mu\text{m}$  in length, with trap frequency  $\omega_{\perp}/(2\pi) \simeq 20\text{Hz}$  giving a length unit of  $d_{\perp} \simeq 2.4 \mu\text{m}$ . This would give an annulus with inner and outer radii of  $25 \mu\text{m}$  and  $34 \mu\text{m}$  respectively, and is of interest as it corresponds to feasible parameters in future experiments. Eq. (30) is also plotted in Fig. 4(a), where we see very good agreement with the hydrodynamic results for  $\nu < 40$ .

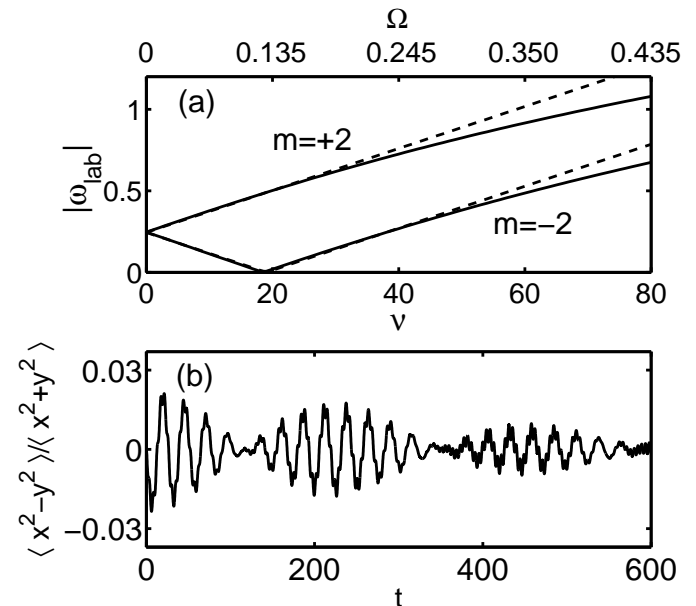


FIG. 4: (a) Frequencies in the laboratory frame of the low-lying  $m = \pm 2$  modes as a function of  $\nu$  and  $\Omega$ , for  $g = 680$  and  $\lambda = 0.00322$ . The solid lines corresponds to numerical solutions of Eq. (24), while the dashed lines show the analytical expression (30) for both modes. (b) The quadrupole moment  $\langle x^2 - y^2 \rangle$  (normalized to the mean squared radius  $\langle x^2 + y^2 \rangle$ ) as a function of time (in units of  $\omega_{\perp}^{-1}$ ) given by a numerical simulation of the GP equation in the laboratory frame. The original condensate contains a single  $\nu = 1$  vortex, and the applied perturbation mainly excites the low-lying  $m = \pm 2$  modes.

Above a particular value of  $\nu$  we find that  $\omega$  of the

$m = -2$  mode becomes negative. From Eq. (30) this critical value is found to be independent of  $|m|$  and given by  $\nu_{\text{crit}} = \eta/(\lambda\sqrt{24})$ , in good agreement with the numerical hydrodynamic results. This corresponds to the point at which the  $m = -|m|$  modes become energetically unstable, whereupon a source of dissipation (such as the presence of a thermal cloud at non-zero temperatures) results in the mode amplitudes increasing with time. This can also be seen from the famous Landau criterion [26], which states that excitations in a superfluid become energetically unstable at flow velocities,  $v$ , exceeding the speed of sound,  $c$ . For a thin annulus surrounding a vortex the fluid velocity is  $v = \nu/R$ , while  $c = \eta/\sqrt{12\lambda}$ , immediately leading to the equation for  $\nu_{\text{crit}}$  derived above.

Another interesting consequence of the fact that the mode frequencies pass through zero is related to a possible experiment where one applies a small, static perturbation of multipolar form to a condensate containing a  $\nu \simeq \nu_{\text{crit}}$  vortex. This is similar to the experiment performed for a vortex lattice in a harmonically-trapped condensate [34], whereupon the negative  $m$  modes are resonantly excited and the resulting non-linear behavior studied.

An important question relates to the feasibility of exploiting the splitting between the positive and negative mode frequencies as a diagnostic for the presence of a vortex, in analogy with the similar use of the surface mode splitting in harmonically-trapped condensates [28, 29, 30]. We test this idea in more detail by performing numerical simulations based on the time-dependent GP equation. We start with a condensate with the above parameters, and with a  $\nu = 1$  vortex in the center. A perturbation is added to the lab. frame trap potential of the form  $\delta V = \alpha(x^2 - y^2)$  up to  $t = 1$ , after which the potential is returned to its original form. The subsequent oscillations are tracked by calculating various moments of the system  $\langle \chi \rangle(t) = \int d\mathbf{r} |\Psi(\mathbf{r}, t)|^2 \chi(\mathbf{r})$  as a function of time.

The  $\langle x^2 - y^2 \rangle$  quadrupole moment (normalized to the mean squared radius  $\langle x^2 + y^2 \rangle$ ) is shown in Fig. 4(b) for  $\alpha = 0.0025$ . The perturbation predominately excites the low-lying  $m = +2$  and  $m = -2$  modes [35], and analysis of the time series shows that modes with (lab. frame) frequencies  $\omega = 0.230$  and  $\omega = 0.257$  are present, which agree well with the predictions from the analytical estimate (30) of  $\omega_- = 0.232$  and  $\omega_+ = 0.258$ . Importantly the splittings also closely agree, within 5%, allowing Eq. (30) to be used to deduce  $\nu$  from measurements of the splitting. Physically the frequency splitting is responsible for the “beating” between the two modes evident in the plot in Fig. 4(b). In experiments these modes would be apparent as a density pattern around the annulus, consisting of four antinodes with alternate maxima and minima. The presence of the splitting would then lead to rotation of the position of the antinodes, similar to the “precession” of the quadrupole surface modes seen experimentally in harmonic traps [29, 30]. The precession

frequency  $\omega_{\text{pr}}$  is equal to  $\Delta\omega/(2|m|)$  [26], corresponding to the angular velocity of the reference frame where the modes are degenerate. Note that in the annular condensate the precession frequency is simply

$$\omega_{\text{pr}} = 2\lambda\nu \simeq \Omega, \quad (31)$$

independent of  $|m|$ , in contrast to the harmonically trapped case where the precession frequency depends upon the multipolarity. The second equality is valid for large  $\nu$  and small  $\eta$ , where one can use Eq. (19) with  $E_1 = 1$ . The simulations were repeated for the  $|m| = 1$  modes, as well as the  $|m| = 2$  modes in the presence of a  $\nu = 2$  vortex, yielding frequencies that agree well with the predictions of Eq. (30).

Thus, the splitting of the modes may be observable and should match closely with that found from simple analytical estimates. However, a limiting factor could be the ability of experiments to resolve the density fluctuations associated with the mode, since this would probably be more difficult than observing shape changes as in harmonic traps. One could in principle increase the amplitude of the mode by using a large perturbation (large  $\alpha$ ), but as seen in Fig. 4(b) this can lead to nonlinear coupling of the mode to higher excitations, leading to a rapid damping (note that this damping is absent for smaller perturbations, e.g.  $\alpha = 0.0005$ ). So there is a trade off involved in choosing the size of the perturbation, and this may in practice limit the utility of collective modes for vortex detection.

#### IV. EXPANSION

One alternative to using mode frequencies to detect vorticity in annular condensates was proposed by Tempere *et al.* [17], and involves allowing an expanding condensate to overlap with another expanding condensate without a vortex. The resulting interference pattern reveals the presence of a vortex in the first condensate. However, this method may be difficult to realize experimentally, and a much simpler procedure would be to use only one condensate and allow it to expand freely after switching off the trapping potential. The central question to be addressed in this section is whether imaging the resulting density profile would provide a means to distinguish between states containing a vortex and those without.

We study this question by starting with the GP equilibrium state either with or without a vortex, then propagating the 2D time-dependent GP equation with  $V_{\text{ext}}$  set to zero. We study the narrow annulus case mentioned at the end of the previous section, where  $\lambda = 0.00322$  and  $\eta = 0.3$ . Fig. 5 shows radial cross-sections through the density for  $\nu = 0$ ,  $\nu = 1$  and  $\nu = 2$  for various times during the expansion. Initially at  $t = 0$  (Fig. 5(a)) there is very little difference between the three configurations, illustrating the difficulty in distinguishing between the three states *in-situ*. After release from the trap ( $t > 0$ )

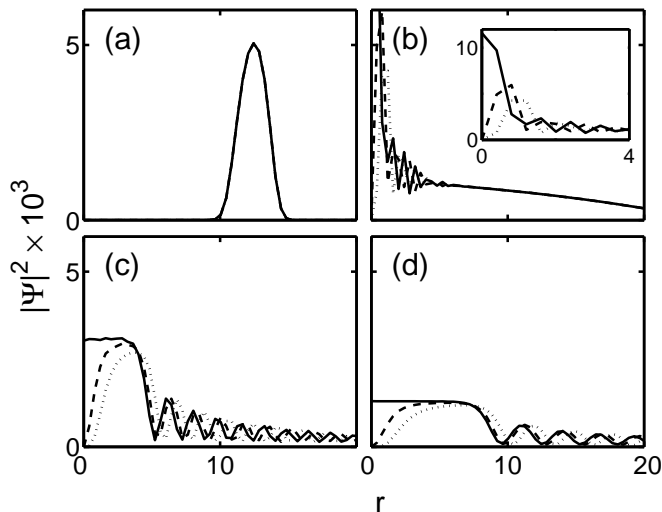


FIG. 5: Density as a function of radial distance through an expanding condensate ( $\lambda = 0.00322$ ,  $\eta = 0.3$ ) with no vortex (solid line), a  $\nu = 1$  singly-quantized vortex (dashed) and a  $\nu = 2$  doubly-quantized vortex (dotted) at (a)  $t = 0$ , (b)  $t = 4$ , (c)  $t = 8$ , (d)  $t = 12$ . The inset in (b) shows the density profiles near to the center, illustrating the differences between the states in this region.

we see that the condensate expands radially both outwards and inwards, thereby filling the annulus. So, even at  $t = 4$  (Fig. 5(b)) the different states are, in principle, distinguishable due to the density hole produced by the centrifugal barrier near to the vortex core. One can also see the development of interference fringes away from the center.

Figs. 5(c) and (d) show the condensate after further expansion. The size of the density dip at the vortex core is proportional to the healing length,  $\xi = 1/\sqrt{2gn}$ , so that the vortex expands along with the condensate due to the corresponding decrease in density. The vortex size can be quantified in the simulations by measuring the width at half the maximum density of the condensate, which for  $\nu = 1$  gives radii of 0.75 at  $t = 8$  and 1.2 at  $t = 12$ . Using the example parameters introduced in the last section, this would correspond to vortex core diameters of  $3.6 \mu\text{m}$  and  $5.6 \mu\text{m}$  at 64 ms and 95 ms respectively, approaching vortex sizes resolvable in experiments [36].

Note that at later times the  $\nu = 0$  condensate density near to the center is relatively uniform, which could provide a means to differentiate between different  $\nu$  states experimentally. For a uniform condensate the radius of the vortex core at half-maximum density can be found numerically [26] yielding values of  $1.5\xi$  and  $3.0\xi$  for  $\nu = 1$  and  $\nu = 2$ . This factor of two difference is reproduced in our simulations, which at  $t = 14$  yield vortex radii at half-maximum of 1.4 and 2.7 for  $\nu = 1$  and  $\nu = 2$  respectively. Using the predicted value  $\xi = 0.9$ , from the measured peak density, yields good estimates for the vortex radii. So in experiments, by measuring the vortex core sizes and using simple theoretical relations, one could

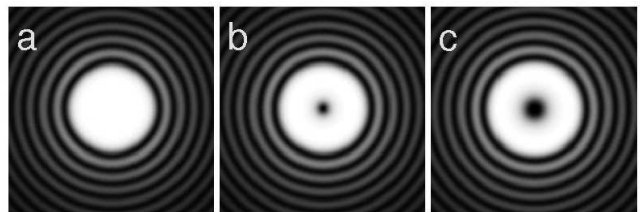


FIG. 6: Density of the expanding condensate ( $\lambda = 0.00322$ ,  $\eta = 0.3$ ) at  $t = 14$  with (a) no vortex ( $\nu = 0$ ), (b) a singly-quantized vortex ( $\nu = 1$ ), and (c) a doubly-quantized vortex ( $\nu = 2$ ). The length scale of each box is  $28 \times 28 d_{\perp}$ .

determine whether either a singly or a doubly quantized vortex is present [37]. In general, the larger the vorticity, the wider will be the central hole at a given instant after release from the trap. However, the quantitative measurement of large vorticity values could in practice be limited by the longer expansion times needed to yield a wide enough central plateau, the corresponding reduction in density making the experimental imaging difficult.

Fig. 6 shows the 2D density profile at  $t = 14$  for  $\nu = 0$ ,  $\nu = 1$  and  $\nu = 2$ , which would be similar to the absorption images typically found in experiments. As well as showing the density profiles are circularly-symmetric, it also illustrates the large differences between the images, which adds qualitative support to the idea that it should be relatively simple to distinguish between different vortex states after expansion.

It is important to note that the central plateau is a consequence of repulsive interatomic forces, and for free expansion with no interactions a more sharply peaked distribution is found. In this latter case the condensate wavefunction is given by the analytical expression [26]

$$\Psi(\mathbf{r}, t) = e^{-iD\pi/4} \left( \frac{M}{2\pi\hbar t} \right)^{D/2} \int \psi(\mathbf{r}', 0) e^{iM(\mathbf{r}-\mathbf{r}')^2/2\hbar t} d\mathbf{r}', \quad (32)$$

where  $D$  is the dimensionality, so in this case  $D = 2$ . Note also that we have returned to using physical units. At large times,  $t \gg MR_+^2/\hbar$ , the density of the expanded condensate is circularly symmetric and tends towards

$$|\Psi(\mathbf{r}, t \rightarrow \infty)|^2 = \left( \frac{M}{\hbar t} \right)^2 \left| \Phi \left( \frac{Mr}{\hbar t} \right) \right|^2, \quad (33)$$

where  $|\Phi(k)|^2$  is the momentum distribution of the condensate. This will be discussed in more detail in the next section.

## V. MOMENTUM DISTRIBUTION

A final method for vortex detection involves considering the momentum distribution of the condensate, which could be probed experimentally by switching off interactions during expansion (e.g. by exploiting a Feshbach resonance) as discussed in the previous section, or by Bragg



spectroscopy *via* the dynamic structure factor [38, 39]. Mathematically, the momentum distribution  $|\Phi(\mathbf{k})|^2$  is obtained by Fourier transforming the equilibrium wavefunction  $\Psi(\mathbf{r}) = |\Psi(r)|e^{i\nu\phi}$ . After integrating over the angular coordinate (i.e. performing a Hankel transform) one obtains

$$|\Phi(k)| = \int_0^\infty dr r |\Psi(r)| J_\nu(kr), \quad (34)$$

where we have taken the modulus to remove constant phase factors, and  $J_\nu(kr)$  is the Bessel function of order  $\nu$ . As we have already seen, for small  $\nu$  one can approximate the equilibrium density in position space with the TF profile (4). In this case the integral can be rewritten in terms of the variable  $\zeta = (r^2 - R_+^2/2)/(R_-^2/2)$  as

$$|\Phi(k)| = \sqrt{\frac{3\eta}{32\pi\lambda}} \int_{-1}^1 d\zeta \sqrt{1-\zeta^2} J_\nu\left(\frac{k\sqrt{1+\eta\zeta}}{\sqrt{2\lambda}}\right). \quad (35)$$

The limit of this integral for a narrow annulus ( $\eta \ll 1$ ) is of particular interest. A series expansion of the Bessel function in powers of  $\eta$  then gives the simple result

$$|\Phi(k)| = \sqrt{\frac{3\pi\eta}{128\lambda}} [J_\nu(kR) + \mathcal{O}(\eta^2)], \quad (36)$$

where  $R = 1/\sqrt{2\lambda}$  is the radius of the annulus. Note that odd powers of  $\eta$  disappear due to parity and that the accuracy of this expansion decreases for large  $k$ .

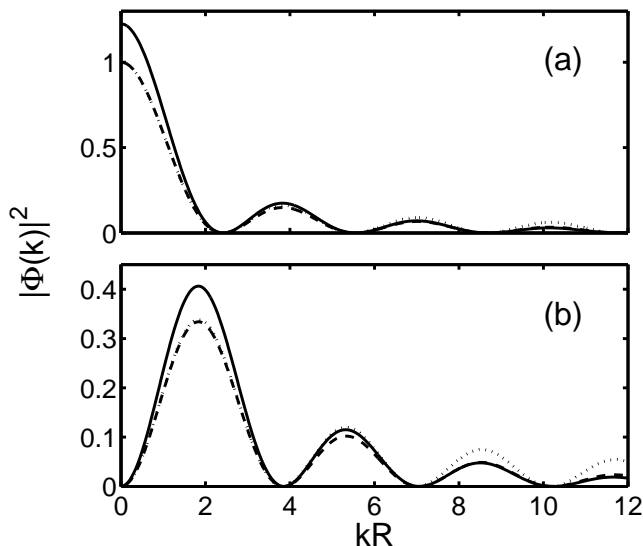


FIG. 7: Scaled momentum distributions  $128\lambda|\Phi(k)|^2/(3\pi\eta)$  as a function of  $kR$  (where  $R = 1/\sqrt{2\lambda}$ ) for (a)  $\nu = 0$ , and (b)  $\nu = 1$  ( $\lambda = 0.00322$ ,  $\eta = 0.3$ ). Solid lines plot the (squared) integral (34) calculated with solutions of the Gross-Pitaevskii equation, while the dashed lines show Eq. (35) for the Thomas-Fermi approximation. For comparison, the squared Bessel functions  $[J_\nu(kR)]^2$  are plotted with dotted lines.

Fig. 7 shows the cylindrically-symmetric momentum distributions  $|\Phi(k)|^2$  for  $\nu = 0$  and  $\nu = 1$  and previously used parameters  $\lambda = 0.00322$ ,  $\eta = 0.3$ . The solid line corresponds to a numerical evaluation of Eq. (34), where the wavefunction is found by solving the time-independent Gross-Pitaevskii equation, while the dashed line plots the TF result (35). These are scaled for comparison to the Bessel function  $J_\nu(kR)$ . One sees that the Bessel function closely approximates the TF result at small momenta, with differences appearing at larger  $kR$ . Further calculations show that the agreement degrades for larger  $\eta$ , as would be expected, although it is still reasonably good for  $kR < 5$ .

There is also a significant difference between the TF and full GP solutions, mostly in the amplitudes of the peaks. This is despite the fact that  $\xi \simeq 0.1d$  so the condition for the validity of the TF approximation is well satisfied. Crucially, however, the positions of the minima and maxima of the momentum distribution are relatively insensitive to the details of the wavefunction. In particular, for both  $\nu = 0$  and  $\nu = 1$  the first few zeros and maxima of  $|\Phi(k)|^2$  from the GP solution agree well with the roots of the corresponding Bessel functions and their derivatives. By virtue of this close correspondence, the positions of these peaks and troughs could provide a means to measure vorticity in experiments. For example, the first maximum could be particularly useful, since its position shifts to higher  $k$  as  $\nu$  increases.

## VI. SUMMARY

We have studied a dilute Bose-Einstein condensate in a “Mexican hat” trapping potential of quartic minus quadratic form. We use the Thomas-Fermi (TF) approximation to analytically find the equilibrium properties of both non-rotating and rotating condensates, and compare to numerical solutions of the Gross-Pitaevskii (GP) equation. In particular, we find that a non-rotating condensate has an annular structure, with a hole in the center, for  $\eta < 1$ , where  $\eta = (12g\lambda^2/\pi)^{1/3}$ . We also find that for condensates in a frame rotating at sufficiently low angular velocities a stable multiply-quantized vortex with circulation  $\nu > 1$  is present at the center. At higher angular velocities our Gross-Pitaevskii simulations show that the ground state can instead consist of a centered multiply-quantized vortex surrounded by rings of singly-quantized vortices, some of which are visible within the annulus.

We have also investigated the dynamics of a condensate with and without a multiply-quantized vortex, particularly the collective modes. A hydrodynamic equation was derived within the TF approximation, with solutions that agree well with the results of evolving the GP equation for large interaction strengths and numbers of atoms where the TF approximation is expected to be valid. We find that for a non-rotating condensate in the limit of a thin annulus ( $\eta \rightarrow 0$ ) the mode

frequencies are  $\omega = \sqrt{j(j+1)}$ , where the number of radial nodes  $j = 0, 1, 2, \dots$  defines families of modes containing different angular quantum numbers  $m$ . In this limit modes with the same  $j$  but different  $m$  are degenerate, but diverge as one increases  $\eta$ . The  $j = 0$  family for  $m > 0$  are low-lying modes corresponding to sound waves directed around the annulus. Thus a simple analytical expression for their frequencies can be derived from  $\omega = cq$ , where  $c = \eta/\sqrt{12\lambda}$  is the speed of sound, and  $q = |m|/R$  with  $R = 1/\sqrt{2\lambda}$  the radius of the annulus, giving  $\omega = |m|\eta/\sqrt{6}$ .

The mode frequencies in the presence of a multiply-quantized vortex were also analyzed, where it was found that the frequency difference between opposite  $m$  modes in the rotating frame is much smaller than the splitting introduced when transforming to the laboratory frame, especially for the low-lying modes. The possibility of using this splitting for experimental detection of vorticity is explored, in particular the excitation of low-lying  $m = \pm 2$  modes in a thin annulus. Although in theory the splitting could be observable as a ‘‘precession’’ of the mode around the annulus, the practicality of this technique may be limited due to the difficulty of observing the associated small density fluctuations. Hence, as an alternative method we also investigated the free expansion of the condensate after release from the trap. We found that the hole in the annulus tends to be filled during the expansion, meaning that a vortex is clearly discernible as a hole in the expanded density profile. As a consequence of the repulsive interactions, the density of the expanded cloud is relatively uniform near to the center, allowing

the width of the vortex core to be used as a measure of the vorticity.

In contrast, when interactions are switched off during the expansion we find that the central density is less uniform, and at long times it tends towards the momentum distribution of the condensate. Since the momentum distribution can be also probed by Bragg spectroscopy, we have explored the possibility of using such a measurement to detect vortex states. We find that for thin annuli in the Thomas-Fermi approximation the distribution takes the form  $|\Phi(k)|^2 \propto [J_\nu(kR)]^2$ . Fourier transforming the stationary solutions of the Gross-Pitaevskii equation changes the amplitudes, but not the positions, of the peaks, potentially allowing the minima of an experimentally measured momentum distribution to be compared to the zeros of the Bessel function in order to distinguish different  $\nu$  states.

Finally, we would like to stress that most of the results obtained in the thin annulus limit are expected to be valid for generic ring-shaped condensates, independent of the specific form of the trapping potential. In particular, near to the minimum a generic Mexican hat potential can be approximated by a harmonic well in the radial coordinate, allowing a precise mapping onto the results for our quartic minus quadratic potential.

#### Acknowledgments

This work was supported by the Ministero dell’Istruzione, dell’Università e della Ricerca.

- 
- [1] M. H. Anderson, J. R. Ensher, M. R. Matthews, C. E. Wieman, and E. A. Cornell, *Science* **269**, 198 (1995).
  - [2] C. C. Bradley, C. A. Sackett, J. J. Tollett, and R. G. Hulet, *Phys. Rev. Lett.* **75**, 1687 (1995).
  - [3] K. B. Davis, M. O. Mewes, M. R. Andrews, N. J. van Druten, D. S. Durfee, D. M. Kurn, and W. Ketterle, *Phys. Rev. Lett.* **75**, 3969 (1995).
  - [4] S. Gupta, K. W. Murch, K. L. Moore, T. P. Purdy and D. M. Stamper-Kurn, *Phys. Rev. Lett.* **95**, 143201 (2005).
  - [5] V. Bretin, S. Stock, Y. Seurin, and J. Dalibard, *Phys. Rev. Lett.* **92**, 050403 (2004).
  - [6] S. Stock, V. Bretin, F. Chevy, and J. Dalibard, *Europhys. Lett.* **65**, 594 (2004).
  - [7] A. L. Fetter, *Phys. Rev. A* **64**, 063608 (2001).
  - [8] E. Lundh, *Phys. Rev. A* **65**, 043604 (2002).
  - [9] K. Kasamatsu, M. Tsubota, and M. Ueda, *Phys. Rev. A* **66**, 053606 (2002).
  - [10] G. M. Kavoulakis and G. Baym, *New J. Phys.* **5**, 51.1 (2003).
  - [11] A. D. Jackson, G. M. Kavoulakis, and E. Lundh, *Phys. Rev. A* **69**, 053619 (2004).
  - [12] A. L. Fetter, B. Jackson, and S. Stringari, *Phys. Rev. A* **71**, 013605 (2005).
  - [13] J. -K. Kim and A. L. Fetter, *Phys. Rev. A* **72**, 023619 (2005).
  - [14] H. Fu and E. Zaremba, cond-mat/0508515.
  - [15] M. Cozzini, A.L. Fetter, B. Jackson, and S. Stringari, *Phys. Rev. Lett.* **94**, 100402 (2005).
  - [16] L. Salasnich, A. Parola, and L. Reatto, *Phys. Rev. A* **59**, 2990 (1999).
  - [17] J. Tempere, J. T. Devreese, and E. R. I. Abraham, *Phys. Rev. A* **64**, 023603 (2001).
  - [18] E. Nugent, D. McPeake, and J. F. McCann, *Phys. Rev. A* **68**, 063606 (2003).
  - [19] A. Aftalion and I. Danaila, *Phys. Rev. A* **69**, 033608 (2004).
  - [20] P. O. Fedichev and G. V. Shlyapnikov, *Phys. Rev. A* **60**, R1779 (1999).
  - [21] P. Rosenbusch, V. Bretin, and J. Dalibard, *Phys. Rev. Lett.* **89**, 200403 (2002).
  - [22] Yu. Kagan, N. V. Prokof’ev, and B. V. Svistunov, *Phys. Rev. A* **61**, 045601 (2000).
  - [23] A. B. Bhattacherjee, E. Courtade, and E. Arimondo, *J. Phys. B: At. Mol. Opt. Phys.* **37**, 4397 (2004).
  - [24] D. S. Petrov, G. V. Shlyapnikov, and J. T. M. Walraven, *Phys. Rev. Lett.* **85**, 3745 (2000).
  - [25] A. Görlitz, J. M. Vogels, A. E. Leanhardt, C. Raman, T. L. Gustavson, J. R. Abo-Shaer, A. P. Chikkatur,

- S. Gupta, S. Inouye, T. Rosenband, and W. Ketterle, Phys. Rev. Lett. **87**, 130402 (2001).
- [26] L. P. Pitaevskii and S. Stringari, *Bose-Einstein Condensation* (Clarendon Press, Oxford, 2003).
- [27] R. J. Donnelly, *Quantized Vortices in Helium II* (Cambridge University Press, Cambridge, 1991).
- [28] F. Zambelli and S. Stringari, Phys. Rev. Lett. **81**, 1754 (1998).
- [29] F. Chevy, K. W. Madison, and J. Dalibard, Phys. Rev. Lett. **85**, 2223 (2000).
- [30] P. C. Haljan, I. Coddington, P. Engels, and E. A. Cornell, Phys. Rev. Lett. **87**, 210403 (2001).
- [31] The  $j = m = 0$  solution is excluded since it does not conserve particle number, and is therefore unphysical.
- [32] The exact solution of Eq. (25) can be formally written as a series expansion in powers of  $\eta$ , i.e.  $\omega_{jm}^2 = \sum_k w_{jmk} \eta^k$ ,  $\delta S_{jm}(\zeta) = e^{im\phi} \sum_k p_{jmk}(\zeta) \eta^k$ , where the functions  $p_{jmk}(\zeta)$  are polynomials of order  $j + k$  and parity  $(-1)^{j+k}$ . Keeping terms up to  $\eta^2$ , for the most interesting cases  $j = 0, 1$  one has  $\omega_{0m}^2 = m^2 \eta^2 / 6$  and  $\omega_{1m}^2 = 2 + (m^2/2 - 3) \eta^2 / 5$ , with the corresponding phase variations  $\delta S_{0m}(\zeta) = [P_0(\zeta) + P_2(\zeta) m^2 \eta^2 / 36] e^{im\phi}$  and  $\delta S_{1m}(\zeta) = [P_1(\zeta) - P_2(\zeta) \eta / 2 + (m^2/4 + 6) P_3(\zeta) \eta^2 / 25] e^{im\phi}$ .
- [33] W. H. Press, B. P. Flannery, S. A. Teukolsky, and W. T. Vetterling, *Numerical Recipes in Fortran* (Cambridge University Press, Cambridge, 1992).
- [34] P. Engels, I. Coddington, P. C. Haljan, and E. A. Cornell, Phys. Rev. Lett. **89**, 100403 (2002).
- [35] At the leading order in  $\eta$  and for small angular velocities, where  $\delta n_{jm}(\zeta) \sim P_j(\zeta) e^{im\phi}$ , the quadrupole operator is  $x^2 - y^2 = [P_0(\zeta) + \eta P_1(\zeta)] \cos(2\phi) / (2\lambda) = (\delta n_{0,+2} + \delta n_{0,-2}) / (4\lambda) + \mathcal{O}(\eta)$ , mainly exciting the ( $j = 0, m = \pm 2$ ) modes. The ( $j = 1, m = \pm 2$ ) modes, whose excitation amplitude is proportional to  $\eta$ , are responsible for the small-amplitude high-frequency oscillations visible in Fig. 4(b).
- [36] K. W. Madison, F. Chevy, W. Wohlleben, and J. Dalibard, Phys. Rev. Lett. **84**, 000806 (2000).
- [37] Experimentally, one could realize a purely 2D expansion by retaining the confinement in the axial direction. A full 3D expansion, inducing a lowering of the effective 2D coupling constant, would enhance the increase of the healing length, changing the scaling of the vortex core radius. However, the qualitative behavior, and in particular the factor of two difference between the vortex radii for  $\nu = 0$  and  $\nu = 1$ , is expected to be preserved.
- [38] J. Stenger, S. Inouye, A. P. Chikkatur, D. M. Stamper-Kurn, D. E. Pritchard, and W. Ketterle, Phys. Rev. Lett. **82**, 4569 (1999).
- [39] F. Zambelli, L. Pitaevskii, D. M. Stamper-Kurn, and S. Stringari, Phys. Rev. A **61**, 063608 (2000).